ISSN: 2181-3337 | SCIENTISTS.UZ VOLUME 5 ISSUE 7 JULY 2026

MATHEMATICAL MODELING OF DEMULSIFIER CONCENTRATION EFFECTS ON OIL–WATER INTERFACIAL TENSION DURING FIELD OIL TREATMENT

Sattorov Mirvohid Olimovich
Associate Professor, Department of Oil and Gas affair, Bukhara state technical university

DOI: 10.67620/sai.57a0011

ABSTRACT
Stable water-in-oil emulsions increase the hydraulic, separation, and chemical-treatment burden of field oil treatment systems. This study develops a statistically evaluated, physically bounded correlation between demulsifier concentration and oil–water interfacial tension (IFT), while explicitly separating that correlation from unvalidated claims about droplet diameter, coalescence rate, or equipment optimization. Fourteen secondary concentration–IFT data pairs (0–210 g/t) attributed to published field-oriented measurements were analyzed using a three-parameter asymptotic exponential model, $\sigma(C) = \sigma_\infty + (\sigma_0 - \sigma_\infty)\exp(-kC)$. Nonlinear least-squares estimation gave $\sigma_0 = 45.81$ mN/m, $\sigma_\infty = 13.18$ mN/m, and $k = 0.01737$ (g/t)$^{-1}$. Model performance was $R^2 = 0.973$, RMSE = 1.59 mN/m, and MAE = 1.40 mN/m. A normalized response function shows that 80%, 90%, and 95% of the modeled attainable IFT reduction are reached at approximately 92.7, 132.6, and 172.5 g/t, respectively. Thus, 100–130 g/t corresponds to about 82.4–89.5% of the modeled IFT response and can be treated as a practical screening band for diminishing returns under the analyzed conditions, not as a universal techno-economic optimum. The model is suitable as a concentration-dependent IFT submodel within broader population-balance, coalescence, settling, or electrostatic-dehydration simulations, provided those models independently represent droplet-size evolution and process hydrodynamics. The work also identifies the validation data required before the correlation can be used for field optimization.

ACCEPTED

07.08.26

Keywords: *field oil treatment; water-in-oil emulsion; demulsifier; interfacial tension; nonlinear regression; diminishing returns; population balance model; electrostatic dehydration.*



1. Introduction

Water-in-crude-oil emulsions are generated when produced water and crude oil are dispersed under shear through chokes, valves, pumps, pipelines, and other flow restrictions. Their persistence is governed by the properties of the oil–water interface, including naturally occurring surface-active material such as asphaltenes and resins, interfacial-film rheology, dispersed-droplet size distribution, temperature, viscosity, brine chemistry, solids, and flow history (Kokal, 2005; Langevin et al., 2004; Raya et al., 2020). Stable emulsions complicate transportation and field treatment because water must ultimately be removed while meeting product-quality, corrosion, and downstream-processing constraints.

Chemical demulsifiers are widely used to accelerate phase separation. Their action is commonly associated with competitive adsorption at the interface, displacement or reorganization of natural stabilizers, modification of interfacial-film properties, and changes in interfacial tension and film-drainage

behavior (Alao et al., 2021; Alara et al., 2022; Rondón et al., 2008). However, interfacial tension alone is not a complete mechanistic description of demulsification. Interfacial viscoelasticity, adsorption kinetics, collision frequency, film drainage, temperature, continuous-phase viscosity, water fraction, and demulsifier chemistry also influence whether colliding droplets coalesce (Langevin et al., 2004; Saad et al., 2019). Recent experimental work nevertheless confirms that IFT can be a useful parameter for assessing demulsifier performance when interpreted together with separation behavior rather than as a stand-alone predictor (Freitas et al., 2025).

Mathematical descriptions of water-in-oil separation range from empirical correlations to population-balance and multiphase-flow models. Population-balance formulations explicitly track droplet birth, coalescence, breakup, settling, and size distributions and therefore provide a physically appropriate framework for predicting actual droplet-size evolution (Cunha et al., 2008; Kooti et al., 2023; Sharma & Thaokar, 2023; Su et al., 2023). Separator-scale simulations similarly demonstrate that droplet-size distribution and emulsion rheology must be coupled to hydrodynamics to predict separation efficiency (Oshinowo & Vilagines, 2020). Electrostatic coalescence introduces additional dependencies on electric-field strength, frequency, dielectric properties, and droplet interactions (Mhatre et al., 2015).

The earlier manuscript on which the present study is based correctly identified a strong concentration dependence of IFT, but it treated a qualitative diameter transformation as if it could directly predict droplet formation, coalescence, settling, and equipment optimization. It also contained calculated IFT values that were inconsistent with its own fitted equation. The revised study therefore narrows the quantitative claim to what the available data actually support: a concentration-dependent IFT submodel and a transparent diminishing-returns analysis.

Accordingly, the objectives are to (1) fit a physically bounded three-parameter exponential relation between demulsifier concentration and IFT; (2) report reproducible goodness-of-fit statistics and parameter uncertainty; (3) correct the tabulated predictions; (4) quantify saturation and diminishing returns without presenting them as a universal economic optimum; and (5) define how the correlation can be incorporated into a broader droplet-coalescence or separator model without conflating IFT with actual droplet diameter.

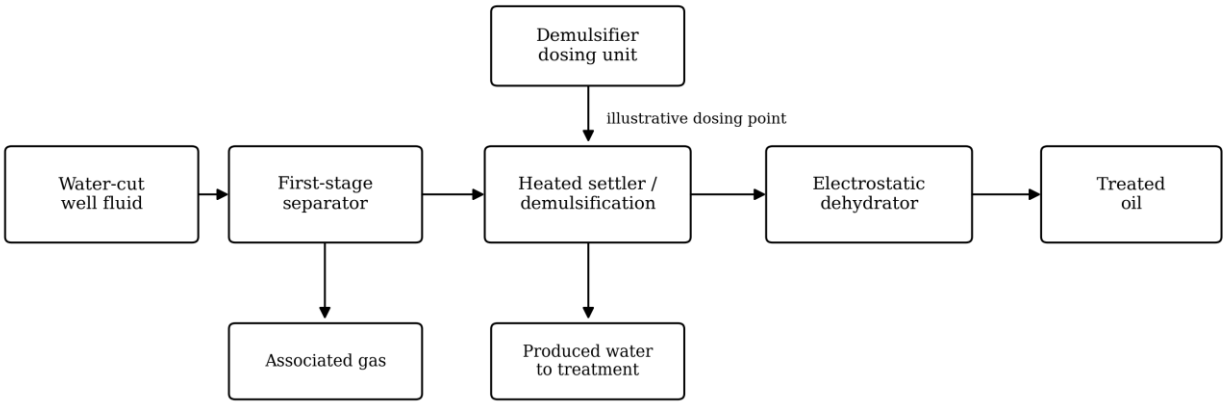


Figure 1. *Conceptual field-oil-treatment arrangement showing an illustrative demulsifier dosing point. The present concentration model informs chemical-dose screening only; the dosing location and equipment design are not optimized by the model.*

2. Materials and Methods

2.1 Data source and study scope

The analysis uses 14 demulsifier-concentration and IFT pairs reproduced in the source manuscript and attributed to Golubev and Khalikova (2004). The cited source describes stalagmometric measurements for a crude-oil emulsion from the Vvedenovskoye field and reports a concentration–IFT curve together with a fifth-order polynomial representation. Because primary instrument records, replicate measurements,

ISSN: 2181-3337 | SCIENTISTS.UZ

and pointwise measurement uncertainties are not available here, the numerical pairs are treated as secondary data rather than as newly generated experimental observations. The analyzed concentration range is 0–210 g/t, and the measured IFT values range from 45.0 to 12–13 mN/m. Equal weighting was used in regression because the source does not report heteroscedastic measurement variances for the reconstructed points. Consequently, the confidence intervals reported below describe regression-parameter uncertainty conditional on this dataset; they do not replace instrument or sampling uncertainty.

2.2 Exponential concentration–IFT model

A monotonic asymptotic exponential model was selected because it represents a rapid initial IFT response followed by saturation and remains bounded at high concentration. Unlike a high-order polynomial, the form does not diverge or oscillate when extrapolated beyond the calibration range. All three parameters were estimated from the data; therefore, the model is explicitly described as a three-parameter model.

$$\sigma(C) = \sigma_\infty + (\sigma_0 - \sigma_\infty) \exp(-kC) \quad (1)$$

where C is the demulsifier concentration (g/t, as reported by the source study), σ(C) is the oil–water interfacial tension (mN/m), σ_0 is the fitted IFT at zero demulsifier, σ_∞ is the asymptotic IFT at high concentration, and k is the empirical concentration-response coefficient, $(g/t)^{-1}$.

2.3 Parameter estimation and goodness of fit

The parameters were estimated by nonlinear least squares. Goodness of fit was evaluated using the coefficient of determination (R^2), root-mean-square error (RMSE), and mean absolute error (MAE). Approximate 95% confidence intervals were calculated from the nonlinear least-squares covariance matrix using a t multiplier with 11 residual degrees of freedom. The calculations were reproduced in Python using nonlinear least-squares routines.

2.4 Diminishing-return metrics

To avoid presenting the fitted curve as a techno-economic optimization that the available data cannot support, a normalized IFT-response fraction was defined. This metric expresses how much of the total model-predicted reduction between σ_0 and σ_∞ has been achieved at concentration C.

$$R(C) = [\sigma_0 - \sigma(C)] / [\sigma_0 - \sigma_\infty] = 1 - \exp(-kC) \quad (2)$$

For a selected response fraction f (for example, 0.80, 0.90, or 0.95), the corresponding concentration is:

$$C(f) = -\ln(1 - f) / k \quad (3)$$

The local marginal IFT reduction per unit increase in demulsifier concentration is the magnitude of the derivative of Equation (1):

$$M(C) = -d\sigma/dC = k(\sigma_0 - \sigma_\infty) \exp(-kC) \quad (4)$$

R(C) and M(C) quantify saturation and diminishing returns, but neither includes chemical price, oil value, residual-water penalties, residence time, throughput, temperature, or other process constraints. They are therefore screening metrics, not an economic objective function.

2.5 Boundary between the IFT submodel and droplet-separation models

The model does not convert IFT directly into actual droplet diameter. Actual droplet growth requires a coalescence model, droplet-size population balance, or experimental droplet-size data. Once an actual or predicted droplet diameter d is available, gravitational settling may be estimated under Stokes-regime assumptions by:

$$v = \Delta\rho \, g \, d^2 / (18 \, \mu) \quad (5)$$

where v is settling velocity, Δρ is the density difference between the phases, g is gravitational acceleration, and μ is continuous-phase viscosity. Equation (5) demonstrates why actual droplet size must be obtained independently: settling velocity scales with d^2. Population-balance and electrocoalescence studies explicitly model the droplet-size distribution and collision/coalescence mechanisms required for such predictions (Cunha et al., 2008; Kooti et al., 2023; Sharma & Thaokar, 2023; Su et al., 2023).

ISSN: 2181-3337 | SCIENTISTS.UZ

3. Results and Discussion

3.1 Fitted parameters and statistical performance

The fitted parameter values are summarized in Table 1. The model predicts $\sigma_0 = 45.81$ mN/m and an asymptotic high-concentration value $\sigma_\infty = 13.18$ mN/m. The response coefficient is $k = 0.01737$ $(g/t)^{-1}$. The fitted zero-concentration value is close to the observed 45.0 mN/m without being artificially constrained to pass through that point. The asymptote is consistent with the observed flattening of the dataset at high concentration.

Table 1. *Three-parameter exponential-model estimates and fit statistics*

Quantity	Estimate	Standard error	Approx. 95% CI	Unit
σ_0	45.81	1.55	42.39 to 49.23	mN/m
σ_∞	13.18	1.25	10.43 to 15.92	mN/m
k	0.01737	0.00238	0.01213 to 0.02260	$(g/t)^{-1}$
R^2	0.973	—	—	dimensionless
RMSE	1.59	—	—	mN/m
MAE	1.40	—	—	mN/m

The fitted equation is therefore $\sigma(C) = 13.18 + 32.63 \exp(-0.01737C)$, mN/m. It explains approximately 97.3% of the variance in the secondary dataset, with RMSE = 1.59 mN/m. Figure 2 shows that the fit captures the overall monotonic decrease and high-concentration plateau. The residual pattern includes several positive residuals between approximately 110 and 160 g/t and negative residuals near 65–80 and 190–210 g/t, so the model should be treated as a compact empirical correlation rather than a mechanistic law.

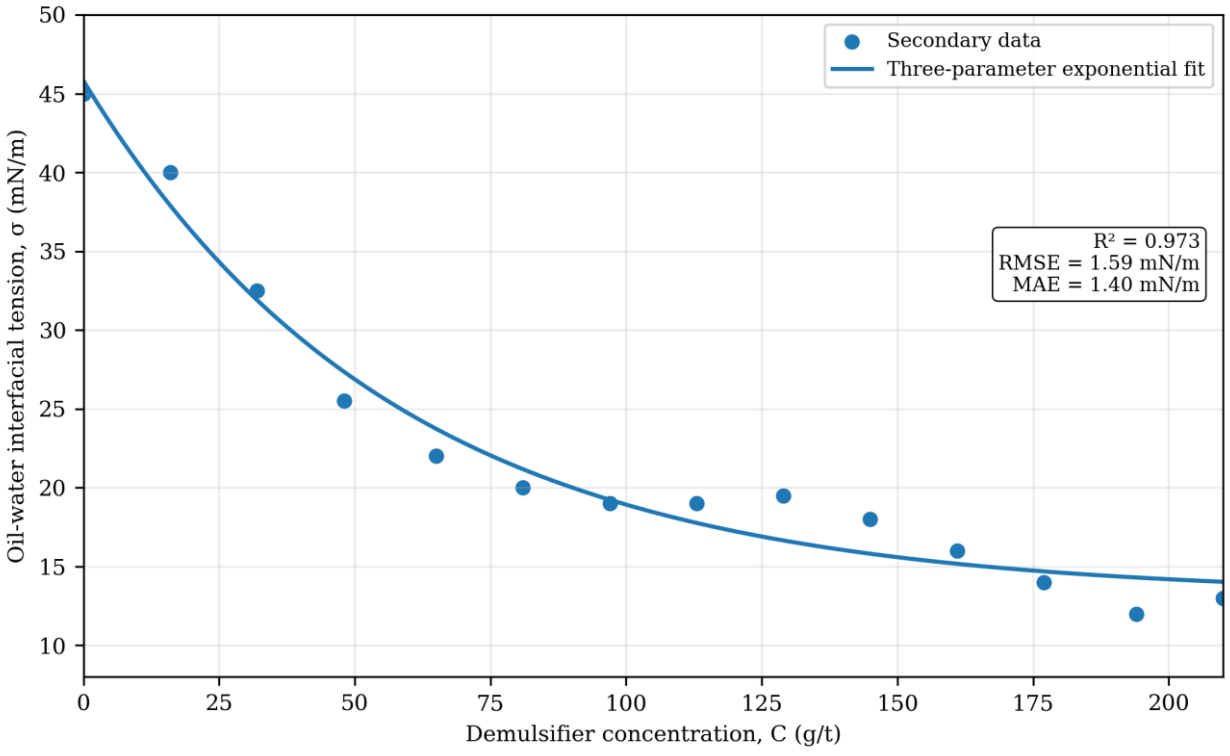


Figure 2. *Secondary interfacial-tension data and fitted three-parameter exponential model.*

3.2 Corrected calculated values

Table 2 regenerates all calculated IFT values directly from the fitted equation. This removes the internal inconsistency in the earlier manuscript, where the calculation column did not correspond to the stated fitted equation. The largest absolute residual in the present table is below 3 mN/m, and the table is numerically consistent with Equation (1).

ISSN: 2181-3337 | SCIENTISTS.UZ

Table 2. *Observed and model-calculated interfacial tension values*

C (g/t)	Observed σ (mN/m)	Calculated σ (mN/m)	Residual: observed − calculated (mN/m)
0	45.0	45.81	-0.81
16	40.0	37.89	+2.11
32	32.5	31.90	+0.60
48	25.5	27.36	-1.86
65	22.0	23.73	-1.73
81	20.0	21.17	-1.17
97	19.0	19.23	-0.23
113	19.0	17.76	+1.24
129	19.5	16.65	+2.85
145	18.0	15.81	+2.19
161	16.0	15.17	+0.83
177	14.0	14.69	-0.69
194	12.0	14.30	-2.30
210	13.0	14.03	-1.03

3.3 Saturation and diminishing returns

Equation (2) provides a transparent way to quantify where the response begins to saturate. The model reaches 80% of its attainable IFT reduction at 92.7 g/t, 90% at 132.6 g/t, and 95% at 172.5 g/t (Figure 3). At 100 g/t, R = 82.4%; at 130 g/t, R = 89.5%. Thus, the previously discussed 100–130 g/t interval can be retained only as a model-based screening band in which roughly 82–90% of the asymptotic IFT response has been realized.

The marginal-response metric leads to the same interpretation. M(0) is 0.567 mN/m per (g/t), whereas M(100), M(130), and M(200) are 0.100, 0.059, and 0.018 mN/m per (g/t), respectively. At approximately 132.6 g/t the model has achieved 90% of its total IFT reduction and the marginal effect has fallen to 10% of its initial value. This is a mathematically defined diminishing-return point, not a proof of minimum operating cost or maximum dehydration performance.

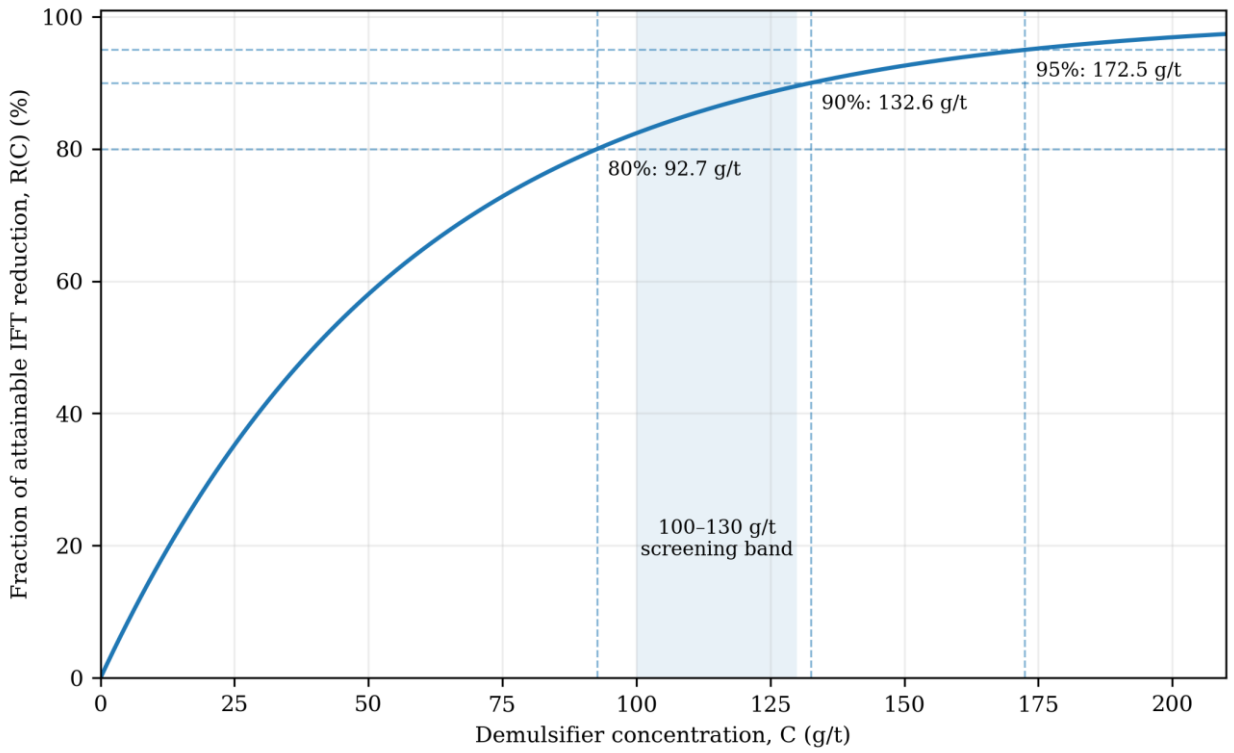


Figure 3. *Modeled fraction of attainable interfacial-tension reduction. The shaded 100–130 g/t region is a screening band for diminishing returns under the analyzed dataset, not a universal economic optimum.*

ISSN: 2181-3337 | SCIENTISTS.UZ

Table 3. *Model-based saturation indicators*

Indicator	Concentration (g/t)	Response achieved	Interpretation
80% response	92.7	80%	Onset of strong saturation
90% response	132.6	90%	Marginal effect ≈ 10% of initial
95% response	172.5	95%	Near-asymptotic response
Screening point	100.0	82.4%	Lower part of practical screening band
Screening point	130.0	89.5%	Upper part of practical screening band

3.4 Engineering interpretation and model boundaries

The correlation is most defensible as a compact computational block that converts demulsifier concentration into an expected IFT for the analyzed crude–water–demulsifier system. Such a block can be called inside a larger simulator that separately calculates droplet collision frequency, film drainage, coalescence efficiency, breakup, settling, residence time, and electrostatic effects. This modular use is consistent with population-balance approaches in which droplet-size evolution emerges from explicit aggregation and transport terms rather than from an assumed proportionality between IFT and diameter (Cunha et al., 2008; Kooti et al., 2023; Sharma & Thaokar, 2023; Su et al., 2023).

The present results do not establish a direct relation between decreasing IFT and decreasing "critical droplet diameter," and no diameter values are reported. This correction is important because the actual size of coalesced water droplets is precisely the quantity that controls settling velocity in Equation (5). Treating a decreasing proxy diameter as an actual droplet diameter would imply slower Stokes settling, contradicting the intended interpretation. A validated model must instead connect interfacial properties to coalescence kinetics and then calculate the evolving droplet-size distribution.

Similarly, Figure 1 should be interpreted as a process-integration schematic rather than an optimization result. The current dataset contains no experimental comparison of injection at the wellhead, upstream of a separator, upstream of a settler, or upstream of an electrostatic dehydrator. Injection-point selection must account for mixing energy, adsorption time, residence time, temperature, water cut, compatibility with other chemicals, and the downstream separation objective. Electrostatic equipment performance also depends on field strength, frequency, dielectric properties, viscosity, water fraction, and droplet interactions (Mhatre et al., 2015).

Finally, the 100–130 g/t range cannot be labeled economically optimal without a cost or performance objective. A genuine techno-economic optimization would require, at minimum, demulsifier cost, dehydration target, residual-water penalty, oil loss, throughput, temperature/energy demand, and residence-time constraints. The present model supplies only the concentration–IFT component of such an objective. Experimental evidence from other crude systems also shows that "optimum" demulsifier dosage depends on crude composition, asphaltene content, diluent, demulsifier formulation, and operating conditions (Rondón et al., 2008; Alara et al., 2022).

3.5 Limitations and validation requirements

First, the model is calibrated to a single secondary dataset derived from a published field-oriented study (Golubev & Khalikova, 2004). It should not be generalized to other crude oils, brines, demulsifier chemistries, temperatures, or water cuts without new calibration.

Second, the source data do not include replicate-level uncertainty. The reported confidence intervals therefore quantify regression uncertainty conditional on the listed points, not total experimental uncertainty. Future measurements should report replicate IFT values, instrument calibration, temperature, fluid composition, and demulsifier identity.

Third, the exponential relation is empirical. It provides a physically plausible monotonic saturation shape but does not resolve adsorption kinetics, interfacial rheology, film drainage, droplet collision

ISSN: 2181-3337 | SCIENTISTS.UZ

efficiency, or coalescence. Recent work indicates that IFT can be informative for demulsifier assessment, but it should be evaluated together with phase-separation performance and other interfacial properties (Freitas et al., 2025; Langevin et al., 2004).

Fourth, no independent validation dataset was available. Before field deployment, the model should be tested prospectively against new concentration–IFT measurements and against dehydration metrics such as separated-water fraction, residual basic sediment and water, droplet-size distribution, and settling time. For equipment-level prediction, those measurements should be linked to population-balance or multiphase models rather than to a direct IFT-to-diameter transformation (Oshinowo & Vilagines, 2020).

4. Conclusions

1. The concentration dependence of oil–water interfacial tension is well represented over 0–210 g/t by the three-parameter exponential relation $\sigma(C) = 13.18 + 32.63 \exp(-0.01737C)$, with $R^2 = 0.973$, RMSE = 1.59 mN/m, and MAE = 1.40 mN/m.

2. All tabulated calculated values have been regenerated directly from the fitted equation, eliminating the numerical inconsistency in the earlier manuscript.

3. Model-based diminishing-return thresholds occur at approximately 92.7 g/t for 80% response, 132.6 g/t for 90% response, and 172.5 g/t for 95% response. The 100–130 g/t interval therefore captures roughly 82–90% of the modeled IFT reduction and may be used as a screening range for the analyzed conditions, not as a universal economic optimum.

4. Interfacial tension is not converted directly into droplet diameter in the revised model. Prediction of actual droplet-size evolution, coalescence rate, and gravitational or electrostatic separation requires an independently formulated population-balance, coalescence, or multiphase model.

5. The fitted $\sigma(C)$ relation can serve as an input block within a broader field-oil-treatment simulator, but field optimization additionally requires validation across fluid compositions and operating conditions, explicit separation-performance data, and a techno-economic objective function.

Data Availability

The complete secondary numerical dataset used for regression is reproduced in Table 2. Its provenance is the concentration–IFT relation attributed to Golubev and Khalikova (2004). No new primary experimental measurements were generated in this modeling study.

REFERENCES

1. Alao, K. T., Alara, O. R., & Abdurahman, N. H. (2021). Trending approaches on demulsification of crude oil in the petroleum industry. Applied Petrochemical Research, 11, 281–293. https://doi.org/10.1007/s13203-021-00280-0
2. Alara, O. R., Abdurahman, N. H., Tade, M. O., Ali, H. A., & Alao, K. T. (2022). Demulsifier: An important agent in breaking crude oil emulsions. Chemical Engineering & Technology, 45(10), 1707–1720. https://doi.org/10.1002/ceat.202100556
3. Cunha, R. E. P., Fortuny, M., Dariva, C., & Santos, A. F. (2008). Mathematical modeling of the destabilization of crude oil emulsions using population balance equation. Industrial & Engineering Chemistry Research, 47(18), 7094–7103. https://doi.org/10.1021/ie800391v
4. Freitas, I. G., Perles, C. E., Guersoni, V. C. B., Pessanha, T. M., & Bannwart, A. C. (2025). Interfacial tension as a parameter to assess demulsifier efficiency on heavy crude oil emulsions. ACS Omega, 10(31), 34142–34150. https://doi.org/10.1021/acsomega.4c06425
5. Golubev, M. V., & Khalikova, A. I. (2004). Optimizatsiya protsessa podachi deemul'gatora [Optimization of the demulsifier injection process]. Neftegazovoe Delo, 2, 80–83. https://www.oil-info.ru/ngd/raz/Golubev_1.pdf
6. Kokal, S. L. (2005). Crude oil emulsions: A state-of-the-art review. SPE Production & Facilities, 20(1), 5–13. https://doi.org/10.2118/77497-PA

ISSN: 2181-3337 | SCIENTISTS.UZ

7. Kooti, G., Dabir, B., Taherdangkoo, R., & Butscher, C. (2023). Modelling droplet size distribution in inline electrostatic coalescers for improved crude oil processing. Scientific Reports, 13, 20209. https://doi.org/10.1038/s41598-023-46251-4
8. Langevin, D., Poteau, S., Hénaut, I., & Argillier, J.-F. (2004). Crude oil emulsion properties and their application to heavy oil transportation. Oil & Gas Science and Technology – Revue d'IFP, 59(5), 511–521. https://doi.org/10.2516/ogst:2004036
9. Mhatre, S., Vivacqua, V., Ghadiri, M., Abdullah, A. M., Al-Marri, M. J., Hassanpour, A., Hewakandamby, B. N., Azzopardi, B. J., & Kermani, B. (2015). Electrostatic phase separation: A review. Chemical Engineering Research and Design, 96, 177–195. https://doi.org/10.1016/j.cherd.2015.02.012
10. Oshinowo, L., & Vilagines, R. D. (2020). Modeling of oil–water separation efficiency in three-phase separators: Effect of emulsion rheology and droplet size distribution. Chemical Engineering Research and Design, 159, 278–290. https://doi.org/10.1016/j.cherd.2020.02.022
11. Raya, S. A., Mohd Saaid, I., Ahmed, A. A., & Umar, A. A. (2020). A critical review of development and demulsification mechanisms of crude oil emulsion in the petroleum industry. Journal of Petroleum Exploration and Production Technology, 10(4), 1711–1728. https://doi.org/10.1007/s13202-020-00830-7
12. Rondón, M., Pereira, J. C., Bouriat, P., Graciaa, A., Lachaise, J., & Salager, J.-L. (2008). Breaking of water-in-crude-oil emulsions. 2. Influence of asphaltene concentration and diluent nature on demulsifier action. Energy & Fuels, 22(2), 702–707. https://doi.org/10.1021/ef7003877
13. Saad, M. A., Kamil, M., Abdurahman, N. H., Yunus, R. M., & Awad, O. I. (2019). An overview of recent advances in state-of-the-art techniques in the demulsification of crude oil emulsions. Processes, 7(7), 470. https://doi.org/10.3390/pr7070470
14. Sharma, E., & Thaokar, R. M. (2023). Population balance modelling of an electrocoalescer. Chemical Engineering Science, 282, 119276. https://doi.org/10.1016/j.ces.2023.119276
15. Su, X., Yang, X., Yu, Y., Gao, F., & Wang, X. (2023). A simulation approach to predict electrostatic coalescence performance of water-in-oil emulsion using population balance model. Separation Science and Technology, 58(3), 538–550. https://doi.org/10.1080/01496395.2022.2131577

ISSN: 2181-3337 | SCIENTISTS.UZ